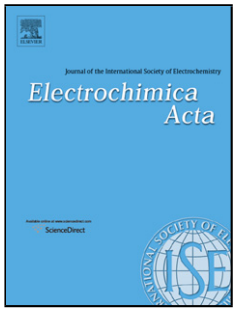


Title: Efficient Photoelectrochemical Reduction of $CO_2$ on Pyridyl Covalent Bonded Ruthenium (II) Based-Photosensitizer

Author: Jibo Liu Huijie Shi Xiaofeng Huang Qi Shen Guohua Zhao

PII: S0013-4686(16)31870-9
DOI: http://dx.doi.org/doi:10.1016/j.electacta.2016.08.135
Reference: EA 27913

To appear in: *Electrochimica Acta*

Received date: 27-6-2016
Revised date: 26-8-2016
Accepted date: 28-8-2016

Please cite this article as: Jibo Liu, Huijie Shi, Xiaofeng Huang, Qi Shen, Guohua Zhao, Efficient Photoelectrochemical Reduction of CO2 on Pyridyl Covalent Bonded Ruthenium (II) Based-Photosensitizer, Electrochimica Acta http://dx.doi.org/10.1016/j.electacta.2016.08.135

# Efficient Photoelectrochemical Reduction of $CO_2$ on Pyridyl Covalent Bonded Ruthenium (II) Based-Photosensitizer

*Jibo Liu, Huijie Shi, Xiaofeng Huang, Qi Shen, Guohua Zhao**

*School of Chemical Science and Engineering, Shanghai Key Lab of Chemical Assessment and Sustainability, Tongji University, 1239 Siping Road, Shanghai 200092, China*

**AUTHOR INFORMATION**

**Corresponding Author**

*G. Zhao. Phone: (+86)21-65981180. Fax: (+86)21-65982287.

E-mail address: g.zhao@tongji.edu.cn

Graphical abstract

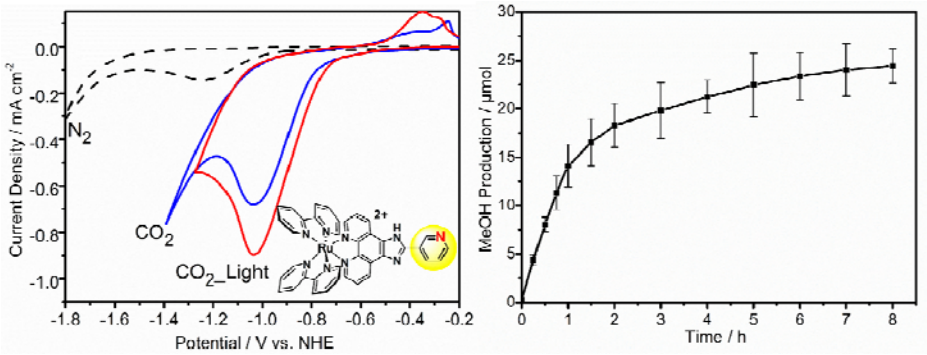

Highlights

- High total faradic efficiency of PEC $CO_2$ conversion was obtained on Ru-Py.
- The catalytic activity of pyridyl for $CO_2$ reduction was well retained.
- The C-C single bond linkage in Ru-Py facilitates methanol production.
- The intermediate pyridiumformate was proved by the simulated reaction.

## ABSTRACT:

Photo/electrochemical $CO_2$ reduction using pyridine was feasible to produce methanol via the formation of pyridiniumformate intermediate. To improve the reduction efficiency, a pyridyl bonded ruthenium (II)-based photosensitizer catalyst (Ru-Py) was designed for photoelectrochemical $CO_2$ conversion. The photocurrent density on Ru-Py modified electrode in $CO_2$ saturated solution was 0.103 mA $cm^{-2}$ higher than that without illumination. The total Faradaic efficiency (f) reached 83.1%, whereas the turnover number (TON) for methanol was 38.4 in aqueous solution after 8 h irradiation. The methanol production was 24.1 μmol which was higher than the published literatures (less than 8 μmol) in similar systems could be attributed to the efficient electron transfer between the photosensitizer and the pyridyl active site covalently linked by C-C bond, as well as the strong and wide absorption up to 610 nm resulted from the large conjugated structure of the ligands. The mechanism investigation revealed that the N atom in pyridyl as catalytic active sites played significant role in $CO_2$ conversion by forming the pyridiniumformate intermediate which was confirmed by the simulation reaction. Meanwhile, in order to realize the reduction process intuitively, the density functional theory (DFT) was applied to

simulate the structure of Ru-Py and the pyridiniumformate intermediates.

***Keyword:*** Ru(II) photosensitizer, Pyridyl catalytic site, $CO_2$ reduction, pyridiniumformate

## 1. Introduction

Carbon dioxide concentration in the air grew rapidly during the past decades due to the excess consumption of fuel resource such as coal, petroleum and natural gas and further caused the resource shortage [1-3]. Efforts has been made to resolve these problems by converting carbon dioxide to higher-energy species such as formic acid, methanol or other clean resource [4-12]. Especially, methanol is an important material for the organic chemical industry and a potential alternative to fossil fuels [13-14]. However, the chemical reduction of $CO_2$ to multi electron reduced liquid product ($CH_3OH$) remains a challenging task [15-16].

Up to now, metal, metal oxide, metal-organic frameworks (MOFs) and metal complexes based catalysts have been designed and synthesized for converting $CO_2$ to desirable products under mild condition [17-26]. Besides, Pyridine is one of the small organic molecules which is able to catalyze the conversion of $CO_2$ to various C1 compounds effectively through multi-electron/proton transfer processes [27-30]. Thanks to the relatively large electronegativity of N atom in pyridine, $CO_2$ could be easily bonded to the molecule and thus be activated [31]. Theoretical calculation has proved that the pyridiniumformate complex (Py-COOH) was a key intermediate for methanol production [32-34]. In 5-10 mM pyridine aqueous solution, pyridine showed efficient catalytic capacity to methanol generation on some noble metal electrodes (Pt,

Pd) due to the surface hydrogen on noble metal [15, 33] and limited kinds of semiconductor electrodes such as n-GaP, p-GaAs and p-InP [29-30, 35]. Pyridine and its derivatives have also been used in photocatalytic system for $CO_2$ reduction by combining with metal organic complex as photosensitizer which exhibited excellent photochemical properties, like suitable redox-properties in both ground and excited state, strong absorption in the visible light region, photochemical stability, and sufficiently long-excited state lifetimes [17-18, 36-37]. MacDonnell and co-workers found that in the catalytic system with $Ru(phen)_3^{2+}$ as photosensitizer and pyridine as catalyst units ($Ru(phen)_3^{2+}$:Py = 1:200), the $CO_2$ reduction efficiency was significantly enhanced, though methanol selectivity was only 0.1% [38]. A ruthenium(II) polypyridyl sensitizer modified with a pyridyl functional group was then developed and a better selectivity (9%) to methanol was achieved in non-aqueous solution because of the more efficient intramolecular electron migration in sensitizer coupled pyridyl system [39]. Not only the catalytic activity was well kept but also some unfavorable characteristics caused by dissociative pyridine was apparently suppressed by covalent chemical bonding pyridyl catalyst to metal complex photosensitizer. However, the prominent disadvantage was that the reaction with this catalyst was only performed in organic solution [17, 21-22]. Besides, the formation of Ru(II) dimer originated from the intermolecular coupling in homogeneous also decreased the utilization ratio of photogenerated electrons [16]. To avoid the dimerization and improve the catalytic stability, immobilization of the photo/electrocatalyst onto electrode surface for photoelectric catalysis application has

also been reported [18, 40].

Hence, in this work, a Ru(II) centered complex $Ru(bpy)_2(PIP)^{2+}$ (bpy = 2-(pyridine-2-yl)pyridine, PIP = 2-(pyridin-3-yl)-1H-imidazo[4,5-f][1,10]phenanthroline) (Ru-Py) was designed and immobilized on the fluorine-doped tin oxide coated glass (FTO) for electrochemical (EC) and photoelectrochemical (PEC) $CO_2$ reduction in aqueous solution, in which Ru(II) bipyridine complex was employed as photosensitizer and un-coordinated pyridyl as catalytic units. In order to keep the independence of the pyridyl catalytic site, a covalent C-C single bonding was designed to connect Ru(II) photosensitizer and pyridyl catalytic site. PEC $CO_2$ reduction was then performed on Ru-Py modified electrode. To elucidate the mechanism of $CO_2$ reduction, the influence of pH value, the role of N atom in pyridyl and the steric hindrance caused by the position of pyridyl-N catalytic sites were all investigated in detail as controlled experiments. Besides, density functional theory (DFT) calculation was also applied to optimize the structure of Ru-Py catalyst and identify the reduction intermediates which was further confirmed by simulation reaction and the possible mechanism was proposed.

## 2. Experimental

### *2.1. Chemicals and Materials*

$RuCl_3.xH_2O$ was purchased from Aladdin Industrial Inc., isonicotinaldehyde (98%) was purchased from J&K Scientific Ltd. 1,10-phenanthroline (99.8%), $H_2SO_4$ (98.3%), $HNO_3$ (68%), 2,2'-bipyridine (99.5%), ammonium acetate (98%), potassium bromide (99.5%), N,N-dimethylformamide (DMF, 99.5%), potassium chloride

(99.5%), sodium hydroxide (99.8%) and ethanol (99.8%) were purchased from Sinopharm Chemical Reagent Co., Ltd., SCRC, China without any further dispose. Note that the ultrapure water with its conductivity reaching 18.2 MΩ cm was used for all the solutions preparation.

*2.2. Synthesis of the Photoelectrocatalyst*

The precursor [$Ru(bpy)_2Cl_2$ (bpy = 2,2′-bipyridine)] was synthesized by the method described in the literature [35] from $RuCl_3.xH_2O$ and 2,2′-bipyridine. The ligand PIP containing the pyridyl active site was obtained via two steps synthesis from 1,10-phenanthroline followed the method described in the literature [41-42]. The detail synthesis procedures were described in supporting information (SI).

The photoelectrocatalyst (Ru-Py) was synthesized by the similar method described in the literature [43] from the precursor and PIP. $Ru(bipy)_2Cl_2$ (240 mg, 0.5 mmol) and PIP (150 mg, 0.5 mmol) was refluxed in $EtOH/H_2O$ (10:1, 5mL) for 5 h under the protection of $N_2$. The crude product was obtained after ammonium hexafluorophosphate (163.0 mg, 1.0 mmol) was added. The solid was purified by silica-gel chromatography (dichloromethane: methanol = 1:0 to 20:1) to give the title compound as a red needle solid (120 mg, yield: 32.7%). The procedures for Ru-Ph and Ru-Py(o)(o: ortho-) were similar with that for Ru-Py. The $^1$HNMR spectra, XPS information and detail synthesis procedures were described in supporting information (Fig. S1-S2, SI).

Ru-Py (4 mg, 0.004 mmol) was added to $CH_3CN$ (1mL) and then Nafion solution (20 μL) was added. The mixture was shaken for 5 mins to get an evenly

solution. 0.5 mL of the solution was dripped slowly to the surface of a FTO with an area of 1 cm × 2 cm and evaporated naturally. The FTO was then washed with deionized water and dried in vacuum at 40 $^{o}$C for 12 hours to obtain a Ru-Py thin film working electrode for PEC reduction.

*2.3. Characterization*

$^{1}$H NMR spectra were obtained on a Bruker AVANCE III 400MHz spectrometer operating at 400 MHz. The electrochemical measurements were obtained on a CHI660C electrochemical workstation (CH Instruments, Inc., USA) using a conventional three-electrode system. The steady-state fluorescence spectra of Ru-Py were recorded on Hitachi, F-7000 fluorescence spectrophotometer. The absorption spectra were measured by an ultraviolet-visible spectrophotometer (UV−Vis, Agilent 8453). The methanol was detected with Agilent GC-MS (6890N Network GC system with a 5973 Network Mass Selective detector) by headspace analysis.

The cyclic voltammetry (CV) measurements in organic phase was recorded in 0.01 mM Ru-Py DMF (containing 1.0 M $H_2O$) solution, 0.1 M [(n-$Bu_4N$)($PF_6$)] was dissolved as supporting electrolyte, glassy carbon working electrode, $AgNO_3$/Ag reference electrode and graphite flake counter electrode. The (CV) measurements in aqueous solution were obtained with the as-prepared electrode coated with Ru-Py as the working electrode, Ag/AgCl filled with saturated KCl as the reference electrode and a graphite flake as the counter electrode to avoid the reduction products reoxidation [18]. $CO_2$ saturated 0.1 M KCl aqueous solution was employed as the supporting electrolyte to stabilize the transition states involving $CO_2$ reduction in

transition-metal complexes coordinating a $CO_2$ ligand [36]. All the potentials were referenced to normal hydrogen electrode (NHE) unless stated otherwise. The amperometric i-t curve was obtained with an interval of 200 s for light on/off under the light intensity of 20 $mW \cdot cm^{-2}$ at a constant potential of -1.0 V (light source: LA-410UV, Hayashi, Japan).

*2.4. PEC Reduction of $CO_2$ and Products Detection*

Controlled potential photoelectrolysis of $CO_2$ was conducted in a 100 mL homemade double-chamber reactor separated with Nafion-117 proton exchange membrane. Typically, 100 mL 0.1 M KCl solution was used as both the anolyte and catholyte electrolyte solution. Before PEC reduction, high purity $CO_2$ (99.99%) gas was bubbled through the KCl solution in the cathode chamber for 40 min at a flow rate of 30 mL $min^{-1}$ to completely remove dissolved oxygen. Under such condition, $CO_2$ reached saturation in the electrolyte, and the concentration of free $CO_2$ was reached 0.037 M with the pH of 4.1. The potential during the photoelectrochemical reduction was kept constant at -1.0 V under 100 mW $cm^{-2}$ irradiation (light source: PLS-SXE300 xenon lamp, Beijing PerfectLight Co., Ltd., China, with AM 1.5 filter).

The reduction products in aqueous phase were determined by Nash's reagent method [18, 44]. Nash reagent was prepared by adding 25.0 g of ammonium acetate, 2.1 mL of acetic acid and 0.2 mL of acetylacetone into water and making the total volume of the solution 100 mL. Then 2.0 mL of liquid sample was mixed with 2.0 mL of Nash reagent and shaken for 1 h at 60 $^{o}$C. The final solution was analyzed by UV-vis spectroscopy and the absorbance at 413 nm was used for quantification (The

standard curve was shown in Fig. S2, SI) to give the amount of formaldehyde ($N_{formaldehyde}$). For detection of the amount of formic acid, 0.5 mL of liquid sample was added into magnesium powder (50 mg) following by drop-wise addition of 0.5 mL 37% hydrochloric acid (10 M) at 0 $^{o}$C and then 3 mL 1 M sodium hydroxide. The resultant suspension was centrifuged at 10 000 rpm for 5 min and 2 mL of supernatant was mixed with 2 mL of Nash reagent and shaken for 1 h at 60 $^{o}$C for UV-vis analysis to determine the total amount of formaldehyde and formic acid ($N_{total}$). The amount of formic acid can be determined after subtracting the amount of formaldehyde in the product ($N_{total}$ - $N_{formaldehyde}$). A headspace GC-MS was used to detect the production of methanol. The chromatographic column (SHRX105MS, 30-m length and 0.5 mm inner diameter) at an oven temperature of 40 °C was employed in combination with a MS detector at 230 °C and helium was the carrier gas. Detection at m/z = 31 was chosen to identify methanol as the reaction products. The samples were preheated at 90 °C in a 20 mL headspace vial with a septa cap, and 1.0 mL of the head space gas was injected from a syringe heated to 90 °C and analyzed in the GC/MS instrument. Control samples containing known concentrations of methanol (in the range 40-280 mM) were analyzed to obtain a standard curve (As shown in Fig. S4, SI). To detect methane, CO and other gaseous product, a thermal couple detector (TCD) and 5 Å molecular filled column equipped Techcomp GC7900 (Techcomp, China) gas chromatogram was employed.

## 3. Results and Discussion

*3.1 EC and PEC Characterization of the Ru-Py Catalyst for $CO_2$ Reduction.*

The electrochemical response of the Ru(II) photoelectron- catalyst were probed by CVs in $N_2$ or $CO_2$-saturated organic media (1M $H_2O$ in DMF ) containing 0.1 M tetrabutylammonium hexafluorophosphate (n-$Bu_4NPF_6$) as supporting electrolyte and 0.1 M KCl aqueous solution respectively. In $N_2$ saturated organic system, Ru-Py undergoes sequential, reversible 1e reductions at $E_{1/2}$ = -0.95 V, -1.14 V and -1.41 V, respectively (Fig. 1a) which arise from 1e reduction of the two bpy ligands and the PIP ligand [45-46]. In $N_2$ saturated aqueous solution, the first two waves coalesced to a single reduction wave with the cathodic peak potential of -1.15 V that arises from the 2e reduction of the 2 bpy ligands (Fig. 1b). In $CO_2$ saturated solution, the reduction waves were enhanced observably, with onset potential at about -1.05 V both in DMF and aqueous solution, indicating the catalytic capability to reduce $CO_2$. To further decrease the reduction potential, the pH adjustment was involved to optimize the $CO_2$ reduction potential in aqueous solution. As shown in Fig. 1b, the onset potential observed for the $CO_2$ reduction shifted positively from -1.05 V to about -0.79 V accompanied with the pH value changing from 7.0 to 5.0. As in more acidic aqueous solution (pH<4), the CVs exhibited obvious irreversible feature (Fig. S5, SI). Upon light irradiation, the peak current density in $CO_2$ saturated aqueous solution at pH 5.0 was 1.3-folds higher than that without irradiation and the onset potential was also positively shifted by 0.05 mV under irradiation. These results suggested that the weakly acidic solution and the introduction of solar light were in favor of $CO_2$ reduction.

The PEC performance of the catalyst Ru-Py was also investigated to illustrate the

photochemical $CO_2$ reduction performance. The cathodic current variation was monitored by amperometric i-t responses recorded at -1.0 V with chopped light irradiation with the title compound loaded on FTO as working electrode. As shown in Fig. 2a, In $N_2$ saturated KCl solution, the photocurrent was also observed due to the light absorbance of Ru(II) photosensitizer and ligand reduction [17]. The electrons in the highest occupied molecular orbital (HOMO) energy level was excited and migrated to the lowest unoccupied molecular orbital (LUMO) energy level due to the solar harvest to generate cathodic photocurrent under bias potential. In $CO_2$ saturated KCl solution, the photocurrent response of cathode increased quickly in 80 s light illuminating duration. This response was attributed to the electrons excitation from HOMO energy level to LUMO energy level after Ru-Py absorbing the optical energy [47]. The increment of current density during the light on/off was about 0.103 mA $cm^{-2}$ which was much higher than that produced on some other material (as shown in table 1) under similar conditions [24, 44, 48-50]. The reason can be attributed to the highly efficient electron migration of the conjugated system. As UV-Vis diffusive reflectance (UV-DRS) result indicated, a broad absorption bands in the visible range was observed for the title complex at wavelength of 300-610 nm attributed to the Ru-N (metal-ligand) transition and π-π* transition (Fig. 2b). Moreover, the increment of photo-current density in $CO_2$-saturated solution were 2.5 folds higher than that in $N_2$ saturated solution, suggesting the title compound was provided with the potential for PEC $CO_2$ reduction.

To investigate the electron transfer route during the $CO_2$ reduction process,

HOMO-LUMO orbital energy level was estimated according to the literatures [51-53]. Using the $Ru^{III/II}$ oxidation potential ($E_{ox}$ vs. NHE), the intersection of the normalized UV-visible absorption spectrum and the photoluminescence, one can evaluate the position of the HOMO and the LUMO energy of the Ru(II) complex based catalyst. The maximum absorption wavelengths of DRS was 40 nm red shift than that UV-vis absorption spectra. The may attributed to the concentration of the two measuring method. In DRS, the intermolecular π-π accumulation greatly promoted the electrons transition and further benefit to absorb long wavelength light [54]. The HOMO orbital energy equals to the $Ru^{III/II}$ redox potential ($E_{ox}$ vs NHE) approximatively. $E_{ox}$ (1.16 V) was estimated from CV which was recorded in 0.05 mM Ru-Py DMF solution with n-$Bu_4NPF_6$ (0.1 M) as supporting electrolyte just as shown in Fig. 3a. The LUMO orbital energy was obtained from the $E_{ox}$ minus the energy gap ($E_{00}$). $E_{00}$ (2.26 V) was calculated based on the equation ($E_{00} = 1240/\lambda$) where the wavelength ($\lambda$ = 548 nm) was estimated from the intersection of normalized UV-visible absorption spectrum and normalized fluorescence spectrum which were detected in 0.05 mM acetonitrile solution as shown in Fig. 3b. As a result, it could be obtained that the energy levels of HOMO and LUMO were loaded at 1.359 eV and -0.901 eV. An enough driving force for the $CO_2$ reduction is achieved because that the reduction potentials for $CO_2$ to methanol (-0.38 eV) and other products are all positive than the energy levels of LUMO (As shown in Fig. 3c). Upon light irradiation, the excited photoelectrons from the HOMO injected into the LUMO through the C-C single bond bridge, and further migrate to the activated $CO_2$.

*3.2. Enhanced PEC $CO_2$ Reduction in Aqueous Solution*

PEC reduction of $CO_2$ was conducted in 100 mL of $CO_2$-saturated 0.1 M KCl aqueous solution under solar light irradiation at −1.0 V. After 8 h irradiation, the liquid products detected in the final products were formic acid and methanol while methane, CO and other compounds were not detected without any gas products detected. The yield of methanol was noticeable though formate acid was the dominant reduction product in the reaction. The Faradaic efficiency ($\eta$) and TON was obtained as the following equations:

$$\eta = (m_p \times n \times F)/(I \times t) \quad (1)$$

$$\text{TON} = m_p/m_{cat} \quad (2)$$

$$\text{TON (in e)} = m_p^e/m_{cat} \quad (3)$$

where $m_p$ is product amount (mol), n is transferred number of electrons, $F$ is Faraday constant (96485.34 $Cmol^{-1}$), $I$ is total observed current (A), $t$ is reaction time (s), $m_p^e$ is electrons migration amount (mol) and $m_{cat}$ is catalyst quantity (mol).

As the desired product, the methanol production was 24.1 μmol (Fig. 4a) with a TON of 3.7 and a Faradaic efficiency of 27.3% under PEC condition. Such a production rate of methanol was quite higher than most reported system under photo/electrode condition containing 10 mM pyridine as shown in table 2 [30-32, 55-56]. In such covalent bonding system, the catalytic activity of the pyridyl was well maintained and the total Faradaic efficiency was 83.1%, which was much higher than that in pyridine and pyridine derivatives on noble metal electrodes system (ranged

from 14% to 51%) [52]. To evaluate the contribution of PC and EC, three parallel reactions were introduced respectively (As shown in table 3). In EC system, 9.3 μmol methanol (TON: 2.4, Faradaic efficiency: 13.2%) was detected while only 2.7 μmol methanol (TON: 0.7) was obtained under PC condition with ascorbic acid (AA) present as electron donor. Only a trace of methanol was obtained under PC condition in the absence of AA, indicating that the plentiful electron supplement was crucial for the $CO_2$ reduction. The yield of the product under EC condition was higher than that under PC condition with AA. It was probably due to the EC process that can supply more electrons than that in PC system whose electron source is sacrificial agent for the reduction reaction. The electrode not only catalyzed the EC conversion of $CO_2$ directly but also functioned as electron source for PC $CO_2$ conversion under PEC condition. The synergistic effect of PC and EC in PEC condition caused 2.5 folds augment for methanol production compared with that in sole PC and EC.

To investigate the crucial active catalytic site of pyridyl in the process of $CO_2$ reduction, Ru-Ph (pyridyl was replaced by benzene) was designed to compare with Ru-Py. The PEC $CO_2$ reduction results found that only 37.2 μmol formic acid was detected after 8 h irradiation at -1.0 V and there was not any methanol (the purple line in Fig. 4b) detected. This indicated that the N atom in pyridyl was essential for the production of methanol. Besides, the result also verified the N atoms in imidazole were not the catalytic active site for the $CO_2$ reduction.

In the photoelectrochemical systems, the pH of the electrolyte solution was an important factor for methanol production. The yield of methanol were 6.2 μmol at pH

= 6.0 (TON: 1.6), 2.9 μmol at pH = 4.0 (TON: 2.9) and 24.1 μmol at pH = 5.0 (TON: 6.4) after 8 h irradiation. As well known, the $pK_a$ of pyridinium ion is 5.3 [31]. The yield of methanol was deeply affected by both the protonated and deprotonated pyridyl for the overall process. To testify the formation of protonated pyridyl, the UV-vis spectrophotometer was employed to detect the absorbance spectra variation at different pH value as shown in Fig. 5a. In the solution of pH = 5.0, the absorbance between 300-400 nm was intense compared with that at pH = 6.0, which corresponding to the low-energy absorption of the metal-to-ligand ($Ru(d_\pi)/PIP(p_{\pi^*})$) charge transition. The absorption change was caused by the protonation of pyridyl (Ru-Py_$H^+$). The formation of Ru-Py_$H^+$ was in favor of the $CO_2$ insertion to produce the pyridiniumformate intermediate (The intermediate was detected by the differential UV-vis absorbance spectra as shown in Fig 5c which would be discussed later) which gave the final product through the further reduction. On the other hand, the solubility of $CO_2$ decreased obviously in strong acidic aqueous solution than that in basic solution. As a result, the optimum methanol production occurring around the $pK_a$ of pyridinium ion (5.3) which was in coincidence with the CVs result.

The electron transfer efficiency between the photo-sensitizer and catalytic site was also an important factor for the $CO_2$ reduction. As literature reported [38], in the non-bridged system [$Ru(phen)_3^{2+}$ photosensitizer with pyridine catalyst], 200-fold amount of catalyst was needed than Ru(II) photosensitizer to capture the photo-generated electrons and only 1.7 μmol methanol was detected. As catalyst was added equally with photosensitizer in the same condition, only 0.17 μmol methanol

was detected. Herein, similar result was also obtained with photosensitizer-catalyst separated system [Ru(II):Py]. The methanol production was 3.8 μmol (TON = 0.8) after 8 hours irradiation at -1.0 V potential. In contrast, the yield of methanol in Ru-Py system were 16 folds than that in [$Ru(phen)_3^{2+}$:Py] system and 7.2 folds than that in[Ru(II):Py] respectively. The highly effective methanol production might be to the more effective electron migration intramolecular than intermolecular. In the photosensitizer bonded catalyst system, the photogenerated electrons of photosensitizer in the excited state transferred to catalytic site (N atom in pyridyl) through the C-C single bond bridging. The intramolecular electron transfer efficiency was much higher than intermolecular. The selectivity to methanol was also increased compared with other system which was also equipped with pyridyl catalytic site. It is more selective for methanol on both an absolute quantum yield basis and relative basis rather than the Ru(II) pyrido-pyrazine catalyst [39] (25.7% of the reducing equivalents end up in methanol for Ru-Py versus 9% for the Ru(II) pyrido-pyrazine catalyst). These comparisons need to be considered with the notion that solvent systems are different in the two cases. The higher methanol selectivity in this system maybe caused by the decreased rigidity of Ru-Py connected by C-C single bond to a certain extent. On the other hand, the independence of pyridyl was well maintained than in the pyrido-pyrazine system.

To evaluate the reduced product caused by the different position of the N atom in pyridyl, Ru-Py(o) was synthesized for $CO_2$ reduction. Headspace GC/MS analysis of aliquots collected after 8 h photoelectrolysis revealed that only 3.7 methanol per

Ru-Py(o) were produced while 6.4 methanol per Ru-Py were produced. The yield of methanol for Ru-Py was 1.7 folds than that for Ru-Py(o). The probable reason could be the unstable pyridiniumformate structure that produced from Ru-Py(o) and activated $CO_2$. The pyridiniumformate internidate formed from Ru-Py and activated $CO_2$ was consummate co-planar surface and all the atoms were in the same plane (Fig 6a) while the intermniadate structure of Ru-Py(o) was unduly tortile (Fig 6b). The DFT optimized pyridiniumformate showed the dihedral angle that built by the $CO_2$ loaded surface and pyridyl loaded was 18$^o$ (angle 2 in Fig. S6) while the dihedral angle that built by the pyridyl loaded surface and phenanthroline loaded was 163$^o$ (angle 1 in Fig. S6). The tension of the tortile intermediate structure caused the instability of the pyridiniumformate and further resulted the decomposition of the intermediate to obtain the 2e product formic acid without deeply reduction to give 6e reduced product.

*3.3 Intermediate Determination and the Plausible $CO_2$ Catalytic Reduction Pathway*

DFT calculations were carried out by using the Gaussian 09 package of programs to further elaborate the feasibility for forming pyridiniumformate as intermediate. B3LYP functional was used with LanL2DZ basis set for Ru atom and 6-31G$^{++}$(d, p) for H, C, N, O atoms [57-61].

The optimized structure of Ru-Py showed that the coordination mode of the Ru atom is regular octahedron with 4 N atoms from two 2,2'- bipyridine and 2 N atoms from ligand PIP. The Ru atom was located at the center of the octahedron while the 6 N atoms was dispersed on the apexes. The length of Ru-N bonds range among 2.102

Å - 2.119 Å. The PIP ligand was fully planar with all the atoms in the same plane to keep the conjugation of the π electrons that in favor of the electron migration from Ru photosensitizer unit to the pyridyl active site. The HOMO of Ru-Py was populated on the uncoordinated pyridyl ring of PIP ligand whereas the LUMO resided primarily on the π system of the bpy moieties (Fig. 6c-d). The carbon atom in $CO_2$ is electropositive and it is beneficial for the $CO_2$ getting close to the pyridyl catalytic site of the Ru(II) complex to form the pyridiniumformate [61]. After Ru-Py was protonated in acidic environment (Ru-Py_$H^+$), the main distribution of the HOMO is the two bpy and the PIP ligand, meanwhile the LUMO of Ru-Py_$H^+$ were mainly distributed on the bpy ligands and the uncoordinated pyridinium ring. The electron density distribution may facilitate electron injecting to the activated $CO_2$ molecule because it provides electronic hybridizing between the photosensitizer and the pyridinium catalytic unit. The calculated LUMO level (-0.72 eV in vacuum, 4.8 eV theoretical absolute potential was used) was also matched with experimental value (-0.91 eV in DMF/$H_2O$). Compared with -0.38 eV ($CO_2$/MeOH theoretical reduction potential), it further demonstrated the electron preferred injection from the photosensitizer to activated $CO_2$ by way of pyridinium catalytic unit.

To futher illustrate the probable mechanism for $CO_2$ reduction, the differential UV-vis absorbance spectra (*ΔA* spectra) was employed to detect the possible intermediates pyridiniumformate in 0.1 M KCl aqueous solution as shown in Fig. 5d. The absorbance of the $CO_2$ saturated aqueous solution was selected as baseline, whose pH value was adjusted to 5.0 by 1 M HCl aqueous solution. Downward peaks

indicated bands disappearing while upward counterparts corresponded to new bands appearing due to photolysis. The change of the absorbance at 364 nm and 520 nm were associated to the formation of key intermediate pyridiniumformate and the dimer $(Ru\text{-}Py)_2$ respectively. The change of the absorbance between 400 - 450 nm attributed to the decomposition of the catalyst [17, 38] and the weakening of M-L bonds by the formation of pyridiniumformate.

The new absorbance bands at 364 nm was caused by the formation of pyridiniumformate intermediate which was the key factor for the production of methanol [39]. To verify the formation pyridiniumformate during the reduction process, a simulate reaction was conducted as follows. Methyl chloroformate which does not display absorbance at 300 - 800 nm in acetonitrile solution (the dash line in Fig. 5b) was employed to simulate the pyridiniumformate because it can easily react with the exposed N atom in pyridyl to give the pyridiniumformate spontaneously without any further processing [62]. The absorbance change of the UV-vis spectra at 340 nm - 400 nm after the addition of the methyl chloroformate can be attributed to the generation of pyridiniumformate (the blue line and the purple line in the Fig. 5b). In contrast, the UV-vis spectra of Ru-Ph had no obvious change after the addition of methyl chloroformate, which indicated the two N atoms in imidazole was difficult to form the formate complex (Fig. 5c). The change of the UV-vis absorption at 340 nm - 400 nm was only caused by the pyridiniumformate that formed by the C-N bond which was composed by the C atom from $CO_2$ and N atom from pyridyl. The time-dependent change of the $\Delta A$ spectra showed the pyridiniumformate increased

continually in the first hour and level off in the next irradiation time (as shown in Fig. 5d). This phenomenon was attributed to the balance of pyridiniumformate formation and dissociation after irradiation for 1 hour. The time-dependent reduced product amount was consistent with the *ΔA* spectra within the same time scale

The absorbance bands at 520 nm attributable to photochemical ligand substitution of the Ru(II) photosensitizer unit giving the corresponding Ru(II) bisdiimine-type complex. This should be a main reason why the rate of photocatalytic production using Ru-Py gradually decreased. Radical dimerization of the Ru(II) photosensitizer unit was reported as the major secondary reaction to quench the photoinduced Ru(II) radical [17]. The upward peaks in Fig. 5e at 520 nm were originated from photochemical ligand substitution of the Ru(II) photosensitizer unit giving that the corresponding Ru(II) bisdiimine-type complex [39]. The dimerization can be avoided effectively by immobilizing the Ru(II) complexes on the surface of FTO electrode during $CO_2$ reduction. Fig. 5e showed the *ΔA* spectra of the Ru(II) photoelectrocatalyst immobilized on the surface of FTO electrode after 10 mins, 1 hour and 8 hours irradiation. The *ΔA* spectra was obtained from comparing the Ru(II) photoelectrocatalyst solutions through soaking the working electrode by ethanol after different irradiation time. Comparing the *ΔA* spectra of immobilized Ru(II) photoelectrocatalyst on the surface of FTO electrode with homogeneous reaction, the disappearance of absorption band at 520 nm indicated that the dimerization was avoided effectively in heterogeneous reaction after the irradiation. Therefore, convenient recycling was another advantage to load the Ru(II) photoelectrocatalyst on

the surface of FTO electrode than diluted in the solution. The absorption bands between 400 - 450 nm correspond to metal-to-ligand charge transfer transition bands (MLCT). As the intermediate formed, the electrons in the Ru(II) photosensitizer migrate to the pyridiniumformate for $CO_2$ reduction thus caused the electron density reduced. The reduced electron density decreased the metal-to-ligand charge transfer which was reflected in the UV-vis absorption [37]. Just as shown in Fig. 5e, the absorption bands between 400 -450 nm was also observed as the Ru-Py loaded on FTO.

Based on the above information, the mechanism of PEC $CO_2$ reduction was proposed in Scheme 1. The first step was the spontaneous protonation of the photoelectrocatalyst to give the protonated compound (Ru-Py_$H^+$) in the weakly acidic solution (pH = 5.0). Subsequently the photo-induced electron of Ru(II) photosensitizer transferred to pyridyl catalytic site through the C-C single bond to obtain the radicals of the catalyst (Ru-Py_$H_0$). The key intermediate (Ru-Py_$H_0$) was formed following the activated $CO_2$ insertion into the N-H bond of Ru-Py_$H_0$, which was detected by UV-vis absorbance. Followed by a series of proton-coupled electron transfer and the release of small molecule, the reduction product such as formic acid, formaldehyde and methanol were generated. Simultaneously, the photoelectrocatalyst was regenerated with the generation of the reduction product.

## 4. Conclusion

Herein, we have designed a covalent C-C bond Ru-Py to convert $CO_2$ to methanol

under PEC system, in which the uncoordinated pyridyl functioned as active site. Different from most of the previous reports in which Ru(II) complex produced 2e transfer product (CO, formic acid), the Ru(II) photosensitizer bonded catalytic active site in this work can convert $CO_2$ to multi-electron reduction products. Uncoordinated pyridyl as the catalytic site in the system showed powerful ability to convert $CO_2$ yielding more valuable products such as methanol due to the rapid intramolecular electron transfer. *ΔA* spectra analysis revealed that the probable reaction route was the formation of pyridinium-formate intermediate from protonated pyridyl complex which was influenced by the pH value. DFT verified that the electron density of HOMO orbital was contributed from the main-ligand containing the uncoordinated pyridyl that in favor of the formation of pyridinium-formate. The yield of the reduction product was influenced by the steric hindrance of the pyridinium-formate intermediate. Although the dimerization of the Ru(II) photoelectrocatalyst was decreased to a limited extent by immobilizing onto the surface of the FTO electrode, the major challenge and the problem urgently to be resolved was the optical instability of the Ru(II) complexes, which limited the extensive using of molecular catalysts.

## ASSOCIATED CONTENT

**Supporting Information**: The detailed information about the ligand synthesis, the $^1H$ NMR Fig. for Ru-Py, Ru-Py(o) and Ru-Ph, the standard curves for formic acid and methanol, and Ru $3d_{3/2}$ XPS spectra. This material is available free of charge via the Internet at http://dx.doi.org/10.1016/j.electacta.

**Notes**

The authors declare no competing financial interest.

**ACKNOWLEDGMENTS**

This work was financially supported by the National Natural Science Foundation of China (NSFC, No. 21477085, 21537003) and Science &Technology Commission of Shanghai Municipality (14DZ2261100).

**REFERENCES**

1. K. Sekizawa, K. Maeda, K. Domen, K. Koike, O. Ishitani, Artificial Z-Scheme Constructed with a Supramolecular Metal Complex and Semiconductor for the Photocatalytic Reduction of $CO_2$. J. Am. Chem. Soc. 135 (2013) 4596-4599.

2. E. E. Benson, C. P. Kubiak, A. J. Sathrum, J. M. Smieja, Electrocatalytic and Homogeneous Approaches to Conversion of $CO_2$ to Liquid Fuels. Chem. Soc. Rev. 38 (2009) 89-99.

3. M. Aresta, A. Dibenedetto, A. Angelini, Catalysis for the Valorization of Exhaust Carbon: From $CO_2$ to Chemicals, Materials, and Fuels. Technological Use of $CO_2$. Chem. Rev. 114 (2014) 1709-1742.

4. H. G. Baldovi, S. Neatu, A. Khan, A. M. Asiri, S. A. Kosa, H. Garcia, Understanding the Origin of the Photocatalytic $CO_2$ reduction by Au- and Cu-Loaded $TiO_2$: A Microsecond Transient Absorption Spectroscopy Study. J. Phys. Chem. C 119 (2015) 6819-6827.

5. C. Kim, H. S. Jeon, T. Eom, M. S. Jee, H. Kim, C. M. Friend, B. K. Min, Y. J. Hwang, Achieving Selective and Efficient Electrocatalytic Activity for $CO_2$ Reduction Using Immobilized Silver Nanoparticles. J. Am. Chem. Soc. 137 (2015) 13844–13850

6. S. Rasul, D. H. Anjum, A. Jedidi, Y. Minenkov, L. Cavallo, K. Takanabe, A Highly Selective Copper-Indium Bimetallic Electrocatalyst for the Electrochemical Reduction of Aqueous $CO_2$ to CO. Angew. Chem., Int. Ed. 54 (2015) 2146-2150.

7. P. Kumar, S. Kumar, S. Cordier, S. Paofai, R. Boukherroub, S. L Jain, Photoreduction of $CO_2$ to Methanol with Hexanuclear Molybdenum $[Mo_6Br_{14}]^{2-}$ Cluster Units under Visible Light Irradiation. Rsc. Adv., 4 (2014) 10420-10423.

8. H. Q. Xu, J. Hu, D. Wang, Z. Li, Q. Zhang, Y. Luo, S. H. Yu, H. L. Jiang, Visible-Light Photoreduction of $CO_2$ in a Metal-Organic Framework: Boosting Electron-Hole Separation Via Electron Trap States. J. Am. Chem. Soc. 137 (2015) 13440-13443.

9. L. Z. Chen, D. D. Huang, J. Z. Ge, F. M. Wang, A Novel Ag(I) Coordination Polymers Based on 2-(Pyridin-4-Yl)-1h-Imidazole-4,5-Dicarboxylic Acid: Syntheses, Structures, Ferroelectric, Dielectric and Optical Properties. Inorg. Chim. Acta. 406 (2013) 95-99.

10. T. Funaki, N. Onozawa-Komatsuzaki, K. Kasuga, K. Sayama, H. Sugihara, New Class of Thiocyanate-Free Cyclometalated Ruthenium(II) Complexes Having a Pyridylquinoline Derivative for near-Infrared Sensitization of Dye-Sensitized Solar Cells. Inorg. Chem. Commun. 35 (2013) 281-283.

11. F. Koschany, D. Schlereth, O. Hinrichsen, On the Kinetics of the Methanation of Carbon Dioxide on Coprecipitated $NiAl(O)_X$. Appl Catal B-Environ 181 (2016) 504-516.

12. D. B. Kayan, F. Koleli, Simultaneous Electrocatalytic Reduction of Dinitrogen

and Carbon Dioxide on Conducting Polymer Electrodes. Appl Catal B-Environ 181 (2016) 88-93.

13. P. Kumar, C. Joshi, N. Labhsetwar, R. Boukherroub, S. L. Jain, A novel Ru/$TiO_2$ hybrid nanocomposite catalyzed photoreduction of $CO_2$ to methanol under visible light. Nanoscale 7 (2015) 15258 - 15267.

14. J. Xiao, D. S. Mao, X. M. Guo, J. Yu, Methanol Synthesis from $CO_2$ Hydrogenation over CuO-ZnO-$TiO_2$ Catalysts: The Influence of $TiO_2$ Content, Energy Technol. 3 (2015) 32 - 39.

15. C. H. Lim, A. M. Holder, J. T. Hynes, C. B. Musgrave, Reduction of $CO_2$ to Methanol Catalyzed by a Biomimetic Organo-Hydride Produced from Pyridine. J. Am. Chem. Soc. 136 (2014) 16081-16095.

16. Y. Yan, E. L. Zeitler, J. Gu, Y. Hu, A. B. Bocarsly, Electrochemistry of Aqueous Pyridinium: Exploration of a Key Aspect of Electrocatalytic Reduction of $CO_2$ to Methanol. J. Am. Chem. Soc. 135 (2013) 14020-14023.

17. A. Nakada, K. Koike, T. Nakashima, T. Morimoto, O. Ishitani, Photocatalytic $CO_2$ Reduction to Formic Acid Using a Ru(II)-Re(I) Supramolecular Complex in an Aqueous Solution. Inorg. Chem. 54 (2015) 1800-1807.

18. X. Huang, G. Zhao, J. Liu, N. Yang, $CO_2$ adsorption-enhanced semiconductor/metal-complex hybrid photoelectrocatalytic interface for efficient formate production, Energy & Environmental Science, (2016) DOI: 10.1039/C6EE00968A.

19. S. Q. Zhang, L. N. Li, S. G. Zhao, Z. H. Sun, J. H. Luo, Construction of

Interpenetrated Ruthenium Metal-Organic Frameworks as Stable Photocatalysts for $CO_2$ Reduction. Inorg. Chem. 54 (2015) 8375-8379.

20. S. Wang, J. Lin, X. Wang, Semiconductor-Redox Catalysis Promoted by Metal-Organic Frameworks for $CO_2$ Reduction. Phys. Chem. Chem. Phys. 16 (2014) 14656-14660.

21. S. Zhang, P. Kang, S. Ubnoske, M. K. Brennaman, N. Song, R. L. House, J. T. Glass, T. J. Meyer, Polyethylenimine-Enhanced Electrocatalytic Reduction of $CO_2$ to Formate at Nitrogen-Doped Carbon Nanomaterials. J. Am. Chem. Soc. 136 (2014) 7845-7848.

22. S. Zhang, P. Kang, T. J. Meyer, Nanostructured Tin Catalysts for Selective Electrochemical Reduction of Carbon Dioxide to Formate. J. Am. Chem. Soc. 136 (2014) 1734-1737.

23. A. Nayak, R. R. Knauf, K. Hanson, L. Alibabaei, J. J. Concepcion, D. L. Ashford, J. L. Dempsey, T. J. Meyer, Synthesis and Photophysical Characterization of Porphyrin and Porphyrin-Ru(II) Polypyridyl Chromophore-Catalyst Assemblies on Mesoporous Metal Oxides. Chem. Sci. 5 (2014) 3115-3119.

24. S. Wang, X. Wang, Photocatalytic $CO_2$ Reduction by CdS Promoted with a Zeolitic Imidazolate Framework. Appl Catal B-Environ. 162 (2015) 494-500.

25. P. Li,; Y. Zhou, Z. Zhao, Q. Xu, X. Wang, M. Xiao, Z. Zou, Hexahedron Prism-Anchored Octahedronal $CeO_2$: Crystal Facet-Based Homojunction Promoting Efficient Solar Fuel Synthesis. J. Am. Chem. Soc. 137 (2015) 9547-50.

26. D. Gao, H. Zhou, J. Wang, S. Miao, F. Yang, G. Wang, J. Wang, X. Bao,

Size-Dependent Electrocatalytic Reduction of $CO_2$ over Pd Nanoparticles. J. Am. Chem. Soc. 137 (2015) 4288-4291.

27. S. Daniel, C. L David, C. P Jonas, Clifford P. K; Reduction of $CO_2$ by Pyridine Monoimine Molybdenum Carbonyl Complexes: Cooperative Metal–Ligand Binding of $CO_2$. Chem. Eur. J. 21 (2015) 8497-8503.

28. E. Lebegue, J. Agullo, M. Morin, D. Belanger, The Role of Surface Hydrogen Atoms in the Electrochemical Reduction of Pyridine and $CO_2$ in Aqueous Electrolyte. Chemelectrochem 1 (2014) 1013-1017.

29. J. A. Keith, E. A. Carter, Theoretical Insights into Pyridinium-Based Photoelectrocatalytic Reduction of $CO_2$. J. Am. Chem. Soc. 134 (2012) 7580-7583.

30. E. E. Barton, D. M. Rampulla, A. B. Bocarsly, Selective Solar-Driven Reduction of $CO_2$ to Methanol Using a Catalyzed P-Gap Based Photoelectrochemical Cell. J. Am. Chem. Soc. 130 (2008) 6342-6344.

31. A. J. Lucio, S. K. Shaw, Pyridine and Pyridinium Electrochemistry on Polycrystalline Gold Electrodes and Implications for $CO_2$ Reduction. J Phys Chem C 119 (2015) 12523-12530.

32. J. H. Jeon, P. M. Mareeswaran, C. H. Choi, S. I. Woo, Synergism between Cdte Semiconductor and Pyridine - Photoenhanced Electrocatalysis for $CO_2$ Reduction to Formic Acid. Rsc Adv 4 (2014) 3016-3019.

33. A. B. Bocarsly, Q. D. Gibson, A. J. Morris, R. P. L'Esperance, Z. M. Detweiler, P. S. Lakkaraju, E. L. Zeitler, T. W. Shaw, Comparative Study of Imidazole and Pyridine Catalyzed Reduction of Carbon Dioxide at Illuminated Iron Pyrite Electrodes. Acs

Catal. 2 (2012) 1684-1692.

34. R. Ma, A. H. Liu, C. B. Huang, X. D. Li, L. N. He, Reduction of Sulfoxides and Pyridine-N-Oxides over Iron Powder with Water as Hydrogen Source Promoted by Carbon Dioxide. Green. Chem. 15 (2013) 1274-1279.

35. M. Lessio, E. A. Carter, What Is the Role of Pyridinium in Pyridine-Catalyzed $CO_2$ Reduction on P-Gap Photocathodes? J. Am. Chem. Soc. 137 (2015) 13248−13251.

36. D. J. Boston, C. Xu, D. W. Armstrong, F. M. MacDonnell, Photochemical Reduction of Carbon Dioxide to Methanol and Formate in a Homogeneous System with Pyridinium Catalysts. J. Am. Chem. Soc. 135 (2013) 16252-16255.

37. Y. J. Sun, Y. Liu, C. Turro, Ultrafast Dynamics of the Low-Lying $^3$MLCT States of $[Ru(bpy)_2(dppp2)]^{2+}$. Chem. Commun. J. Am. Chem. Soc. 132 (2010) 5594-5595.

38. R. Kuriki, K. Sekizawa, O. Ishitani, K. Maeda, Visible-Light-Driven $CO_2$ Reduction with Carbon Nitride: Enhancing the Activity of Ruthenium Catalysts. Angew. Chem., Int. Ed. 54 (2015) 2406-2409.

39. D. J. Boston, Y. M. Pachon, R. O. Lezna, N. R. de Tacconi, F. M. MacDonnell, Electrocatalytic and Photocatalytic Conversion of $CO_2$ to Methanol Using Ruthenium Complexes with Internal Pyridyl Cocatalysts. Inorg. Chem. 53 (2014) 6544-6553.

40. P. Kang, S. Zhang, T. J. Meyer, M. Brookhart, Rapid Selective Electrocatalytic Reduction of Carbon Dioxide to Formate by an Iridium Pincer Catalyst Immobilized on Carbon Nanotube Electrodes. Angew. Chem., Int. Ed. 53 (2014) 8709-8713.

41. X. Wang, J. Zhang, G. Liu, H. Lin, A Series of Cd(II) Complexes with Π–Π

Stacking and Hydrogen Bonding Interactions: Structural Diversities by Varying the Ligands. J Solid State Chem 184 (2011) 280-288.

42. L. Gou, Z. X. Han, H. M. Hu, Q. R. Wu, X. L. Yang, Z. H. Yang, B. C. Wang, F. Wang, M. L. Yang, G. L. Xue, Syntheses and Characterization of Five $d^{10}$ Coordination Polymers Derived from Phenanthroline Derivative and Dicarboxylate Mixed Ligands. Inorg. Chim. Acta 363 (2010) 2590-2599.

43. C. C. Hou, T. T. Li, S. Cao, Y. Chen, W. F. Fu, Incorporation of a $[Ru(Dcbpy)(Bpy)_2]^{2+}$ Photosensitizer and a $Pt(Dcbpy)Cl_2$ Catalyst into Metal-Organic Frameworks for Photocatalytic Hydrogen Evolution from Aqueous Solution. J. Mater. Chem. A 3 (2015) 10386-10394.

44. X. Huang, T. Cao, M. Liu, G. Zhao, Synergistic Photoelectrochemical Synthesis of Formate from $CO_2$ on {121} Hierarchical $Co_3O_4$. J. Phys. Chem. C 117 (2013) 26432-26440.

45. E. Kato, H. Takeda, K. Koike, K. Ohkubo, O. Ishitani, Ru(II)-Re(I) Binuclear Photocatalysts Connected by $-CH_2XCH_2-$ (X = O, S, $CH_2$) for $CO_2$ Reduction. Chem Sci 6 (2015) 3003-3012.

46. P. Kang, Z. F. Chen, M. Brookhart, T. J. Meyer, Electrocatalytic Reduction of Carbon Dioxide: Let the Molecules Do the Work. Top Catal 58 (2015) 30-45.

47. S. Sato, T. Morikawa, S. Saeki, T. Kajino, T. Motohiro, Visible-Light-Induced Selective $CO_2$ Reduction Utilizing a Ruthenium Complex Electrocatalyst Linked to a P-Type Nitrogen-Doped $Ta_2O_5$ Semiconductor. Angew. Chem., Int. Ed. 49 (2010) 5101-5105.

48. Q. Shen, Z. F. Chen, X. F. Huang, M. C. Liu, G. H. Zhao, High-Yield and Selective Photoelectrocatalytic Reduction of $CO_2$ to Formate by Metallic Copper Decorated $Co_3O_4$ Nanotube Arrays. Environ. Sci. Technol. 49 (2015) 5828-5835.

49. Q. Zhai, S. J. Xie, W. Q. Fan, Q. H. Zhang, Y. Wang, W. P. Deng, Y. Wang, Photocatalytic Conversion of Carbon Dioxide with Water into Methane: Platinum and Copper(I) Oxide Co-catalysts with a Core–Shell Structure. Angew. Chem. Int. Ed. 52 (2013) 5776 -5779.

50. R. Lin, L. J. Shen, Z. Y. Ren, W. M Wu, Y. X. Tan, H. R Fu, J. Zhang and L. Wu, Enhanced photocatalytic hydrogen production activity via dual modification of MOF and reduced graphene oxide on CdS. Chem. Commun. 50 (2014) 8533-8535.

51. A. V. Akimov, R. Jinnouchi, S. Shirai, R. Asahi, O. V. Prezhdo, Theoretical Insights into the Impact of Ru Catalyst Anchors on the Efficiency of Photocatalytic $CO_2$ Reduction on $Ta_2O_5$. J. Phys. Chem. B 119 (2015) 7186-7197.

52. A. Sepehrifard, S. G. Chen, A. Stublla, P. G. Potvin, S. Morin, Effects of Ligand Lumo Levels, Anchoring Groups and Spacers in Ru(II)-Based Terpyridine and Dipyrazinylpyridine Complexes on Adsorption and Photoconversion Efficiency in Dsscs. Electrochimica Acta 87 (2013) 236-244.

53. I. M. Dixon, E. Lebon, G. Loustau, P. Sutra, L. Vendier, A. Igau, A. Juris, Broad HOMO-LUMO Gap Tuning through the Coordination of a Single Phosphine, Aminophosphine or Phosphite onto a $Ru(tpy)(bpy)^{2+}$ Core. Dalton T 2008, 5627-5635.

54. G. Konti, E. Chatzivasiloglou, V. Likodimos, G. Kantonis, A. G. Kontos, A. I.

Philippopoulos and P. Falaras, Influence of pyridine ligand nature and the corresponding ruthenium(II) dye molecular structure on the performance of dye-sensitized solar cells. Photochem. Photobiol. Sci., 8 (2009) 726-732.

55. E. B. Cole, P. S. Lakkaraju, D. M. Rampulla, A. J. Morris, E. Abelev, A. B. Bocarsly, Using a One-Electron Shuttle for the Multielectron Reduction of $CO_2$ to Methanol: Kinetic, Mechanistic, and Structural Insights. J. Am. Chem. Soc. 132 (2010) 11539-11551.

56. J. L Yuan, L. Zheng C. J. Hao, Role of pyridine in photoelectrochemical reduction of $CO_2$ to methanol at a CuInS2 thin film electrode, RSC Adv. 4 (2014) 39435-39438.

57. E. B. Cole, M. F. Baruch, R. P. L'Esperance, M. T. Kelly, P. S. Lakkaraju, E. L. Zeitler, A. B. Bocarsly, Substituent Effects in the Pyridinium Catalyzed Reduction of $CO_2$ to Methanol: Further Mechanistic Insights. Top Catal 58 (2015) 15-22.

58. Y. J. Yuan, Z. T. Yu, J. Y. Zhang, Z. G. Zou. A copper(I) dye-sensitised $TiO_2$-based system for efficient light harvesting and photoconversion of $CO_2$ into hydrocarbon fuel, *Dalton Trans.* 41 (2012) 9594–9597.

59. Y. Kuramochi, K. Fukaya, M. Yoshida, H. Ishida, trans-(Cl)-[Ru(5,5′-diamide-2, 2′-bipyridine)$(CO)_2Cl_2$]: Synthesis, Structure, and Photocatalytic $CO_2$ Reduction Activity. Chem.Eur.J. 21 (2015) 10049-10060

60. H. H. Li, Y. Y. Xing, Z. X. Lian, A. W. Gong, H. Y. Wu, Y. Li, Z. R. Chen, Rigidity/flexibility competition in organic/iodoargentate hybrids: a combined experimental and theoretical study. CrystEngComm, 15 (2013) 1721-1728

61. M. Sheng, N. Jiang, S. Gustafson, B. You, D. H. Ess, Y. Sun. A nickel complex

with a biscarbene pincer-type ligand shows high electrocatalytic reduction of $CO_2$ over $H_2O$. Dalton Trans. 44 (2015) 16247-16250.

62. F. Berti, F. Malossi, F. Marchetti, M. Pineschi, A Highly Enantioselective Mannich Reaction of Aldehydes with Cyclic N-Acyliminium Ions by Synergistic Catalysis. Chem. Commun. 51 (2015) 13694-13697.

**Figure Captions**

Fig. 1. (a) Cyclic voltammetry in DMF (containing 1.0 M $H_2O$) under $N_2$ (black) and $CO_2$ (green), 0.1 M [(n-$Bu_4N$)($PF_6$)], 0.01 mM Ru-Py, 50 mVs-1 scan rate, glassy carbon working electrode (area 0.07056 $cm^2$), $AgNO_3$/Ag reference electrode (filled with 10 mM $AgNO_3$ in MeCN, 0.46 V vs. NHE which was calibrated with the Ferrocenium/Ferrocene couple), room temperature. The structure of the Ru(II) photoelectrocatalyst (Ru-Py) was shown in the red square frame; (b) Cyclic voltammetry in water under $N_2$ (black dash line) and 1 atm $CO_2$ at different pH value: pH 7 (green), pH 6 (purple), pH 5 (blue) and pH 5 under visible light irradiation (red). Conditions: 0.1 M KCl aqueous solution, 50 mV $s^{-1}$ scan rate, 0.5 mg Ru-Py loaded FTO as working electrode (area 1.0 $cm^2$), Ag/AgCl reference electrode, room temperature.

Fig. 2. (a) Amperometric i−t curves of Ru-Py (0.5 mg) loaded on FTO in 0.1 M KCl solutions saturated with $N_2$(black) and $CO_2$(red) at −1.0 V with light on/off; (b) UV-vis DRS of the Ru(II) photoelectrocatalyst (Ru-Py).

Fig. 3. (a) CVs in DMF/1.0 M $H_2O$ with 0.1 M (n-$Bu_4N$)($PF_6$) as supporting electrolyte which to detect the $Ru^{III/II}$ oxidation reduction potential (E'); (b) UV-vis Spectra and fluorescence spectra of 0.05M Ru-Py in $CH_3CN$ solution; (c) Energy levels positions of the Ru-Py HOMO-LUMO orbital at pH 5.0 and the redox potentials of $CO_2$.

Fig. 4. (a) Product and TON growth of methanol with irradiation time for Ru-Py and Ru-Py(o); (b) Head space GC/MS analyses for Ru-Py,Ru-Py(o) and Ru-Ph.

Figure 5. (a) UV-visible absorption spectrum of Ru-Py in acetonitrile solution (0.01 M) under different pH value: pH = 6.0 (blue) and pH = 5.0 (red); (b) UV-visible absorption spectrum of Ru-Py acetonitrile solution (red line), 5s after the addition methylic chloroformate (10 equiv; blue line), 60 s after the addition of methylic chloroformate (purple line); (c) UV-visible absorption spectrum of Ru-Ph acetonitrile solution (red line), 5s after the addition methylic chloroformate (10 equiv; blue line), 60 s after the addition of methylic chloroformate (purple line); (d) $\Delta A$ spectra of Ru-Py (22 μM) during PEC system in $CO_2$ saturated 0.1 M KCl aqueous solutions. Peaks pointing down indicate bands disappearing while those pointing up correspond to new bands appearing due to photolysis; (e) $\Delta A$ spectra of the photoelectrocatalyst between before and after irradiation (10 min, 1 h, and 8 h). The solution was obtained by dissolving the photoelectrocatalyst from FTO which was undergoing irradiation.

Fig. 6. The optimized structure of the pyridinium- formate intermediate for (a) Ru-Py and (b) Ru-Py(o). H atoms were hidden in order to show the structure clearly. The electron contribution of Ru-Py for HOMO(c) and LUMO (d). The electron contribution of Ru-Py_H+ for HOMO (e) and LUMO (f).

Scheme 1. Proposed Mechanism for Photoelectrocatalytic $CO_2$ Reduction

Fig. 1.

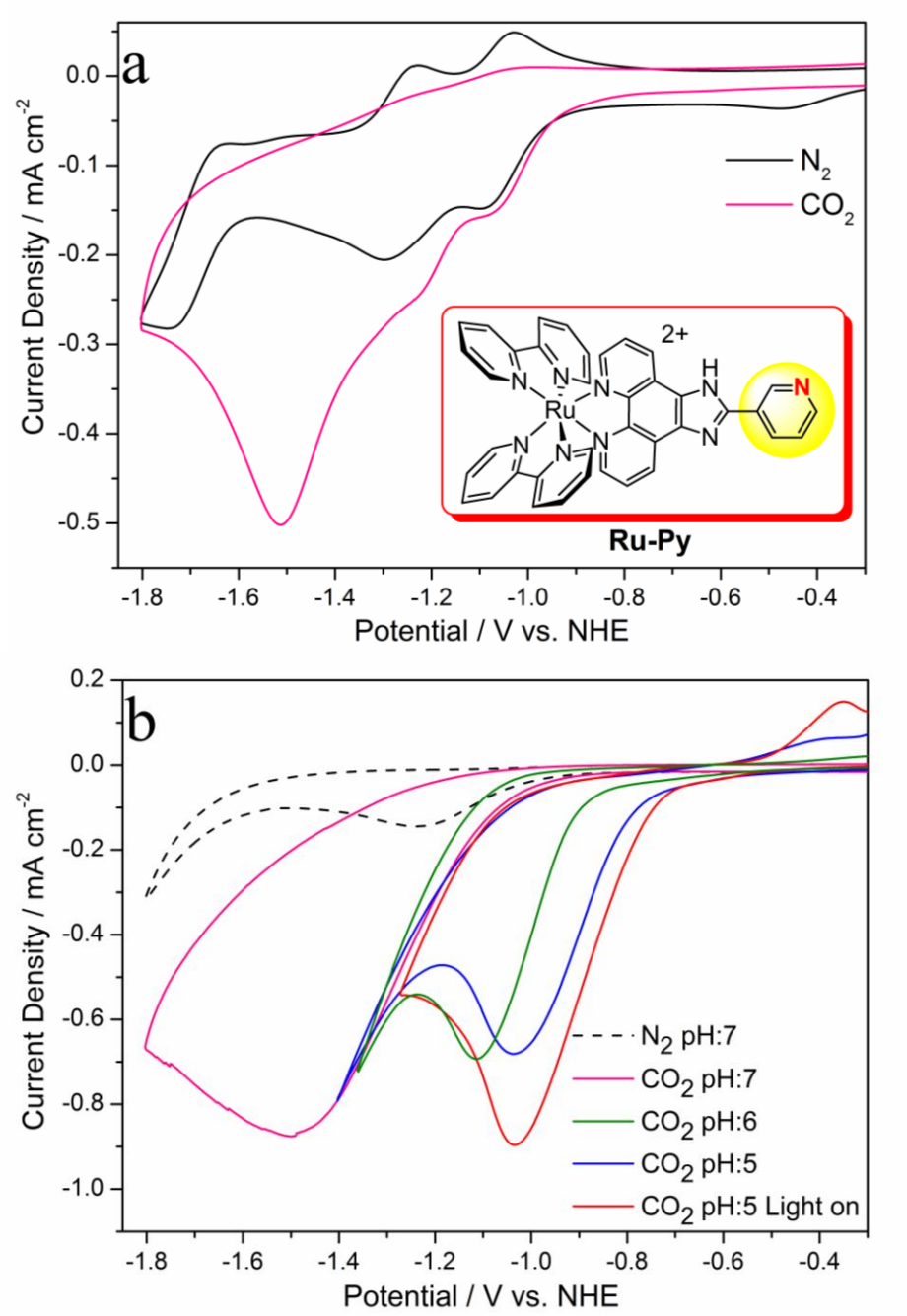

Fig. 2.

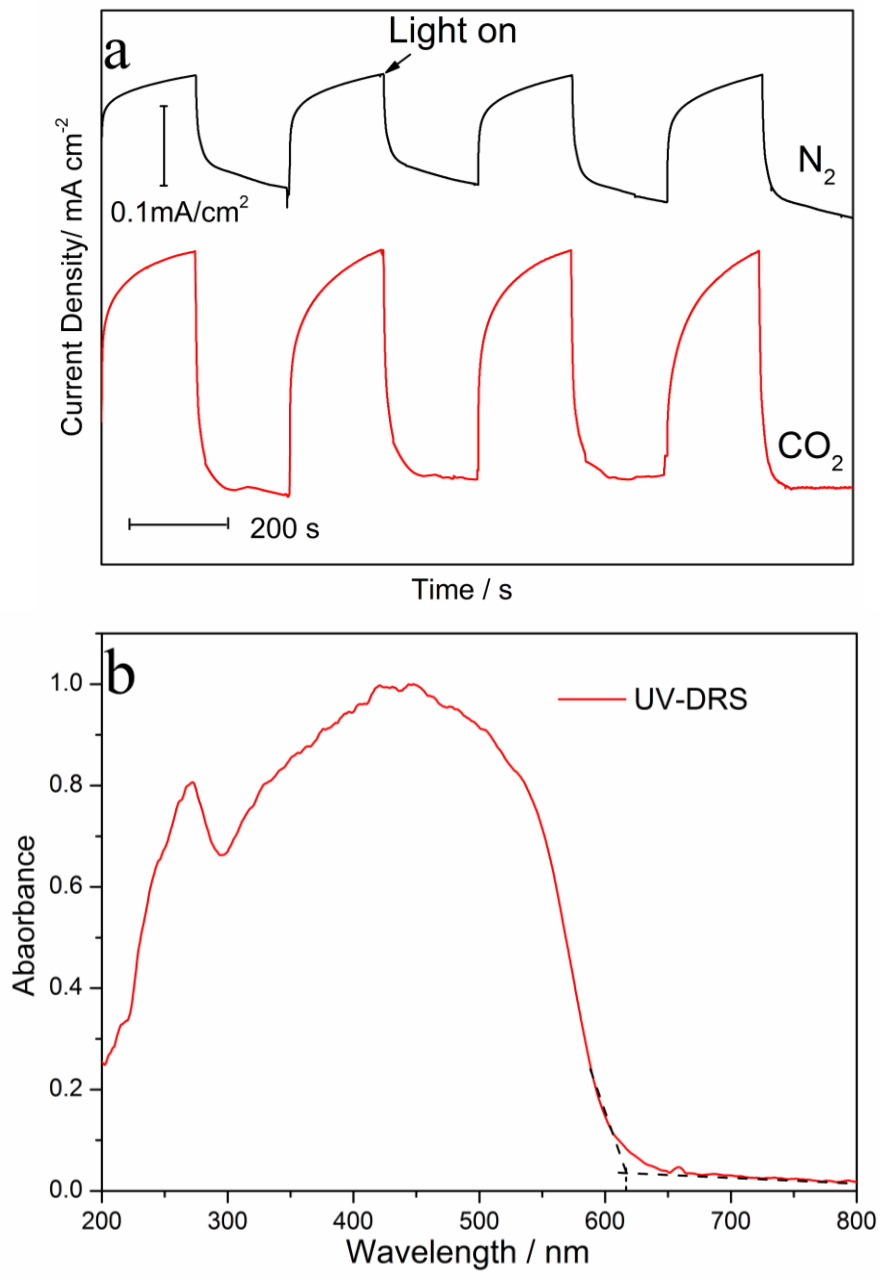

Fig. 3.

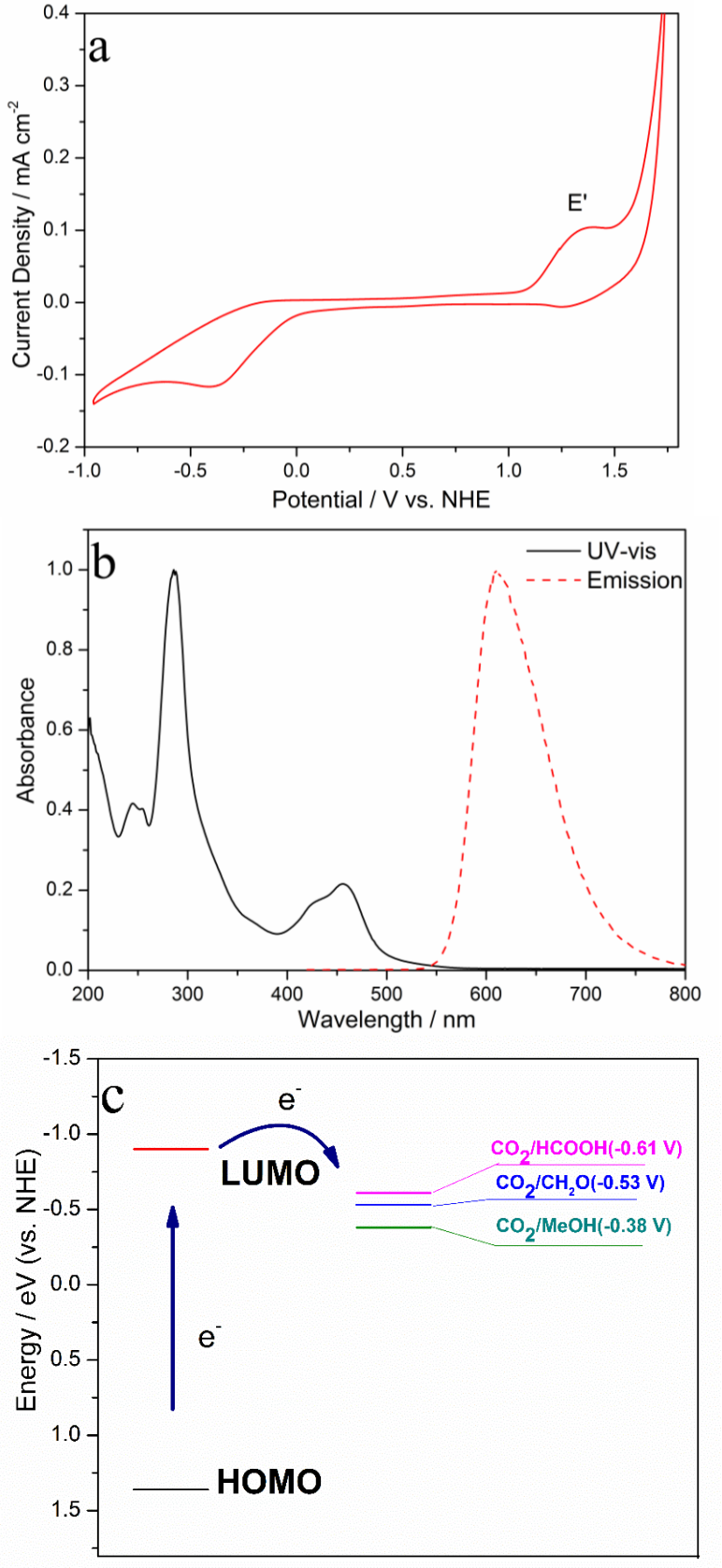

Fig. 4.

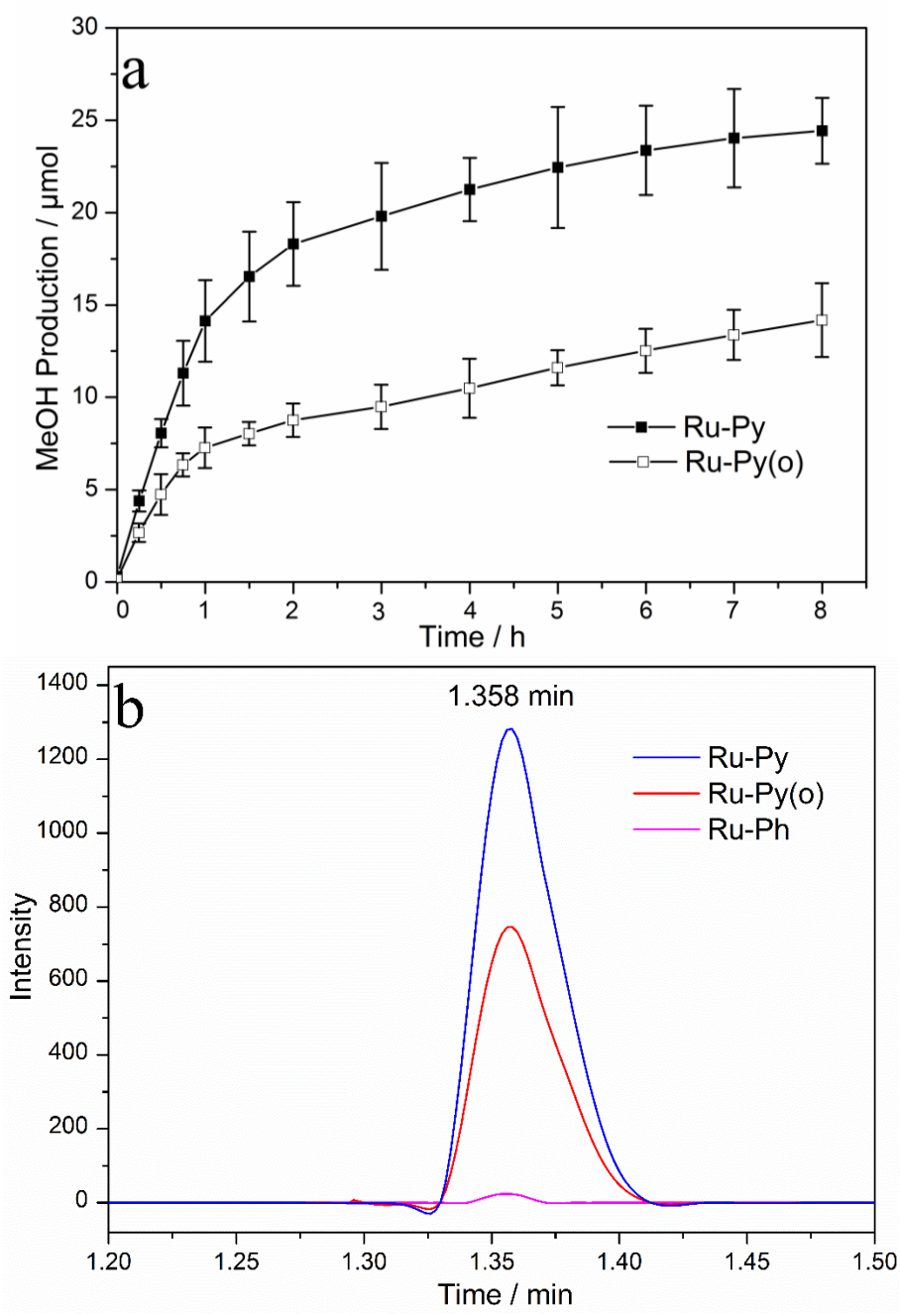

Fig. 5.

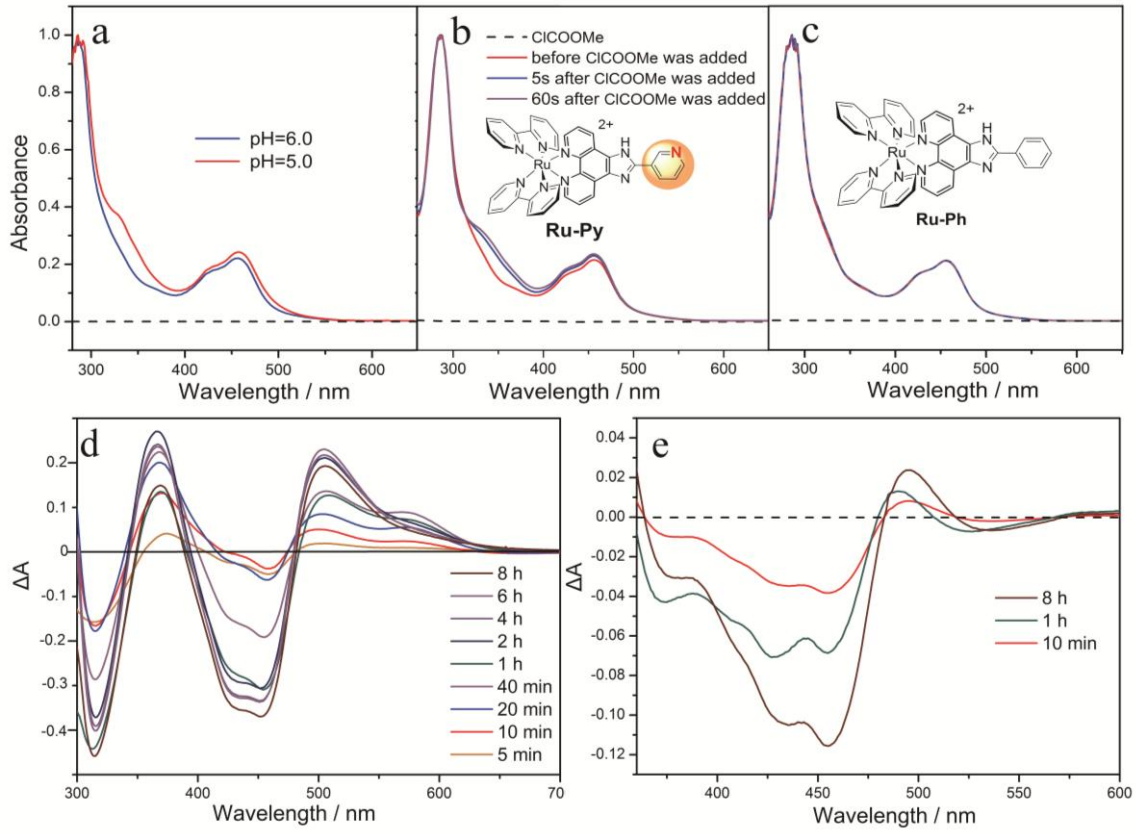

Fig. 6.

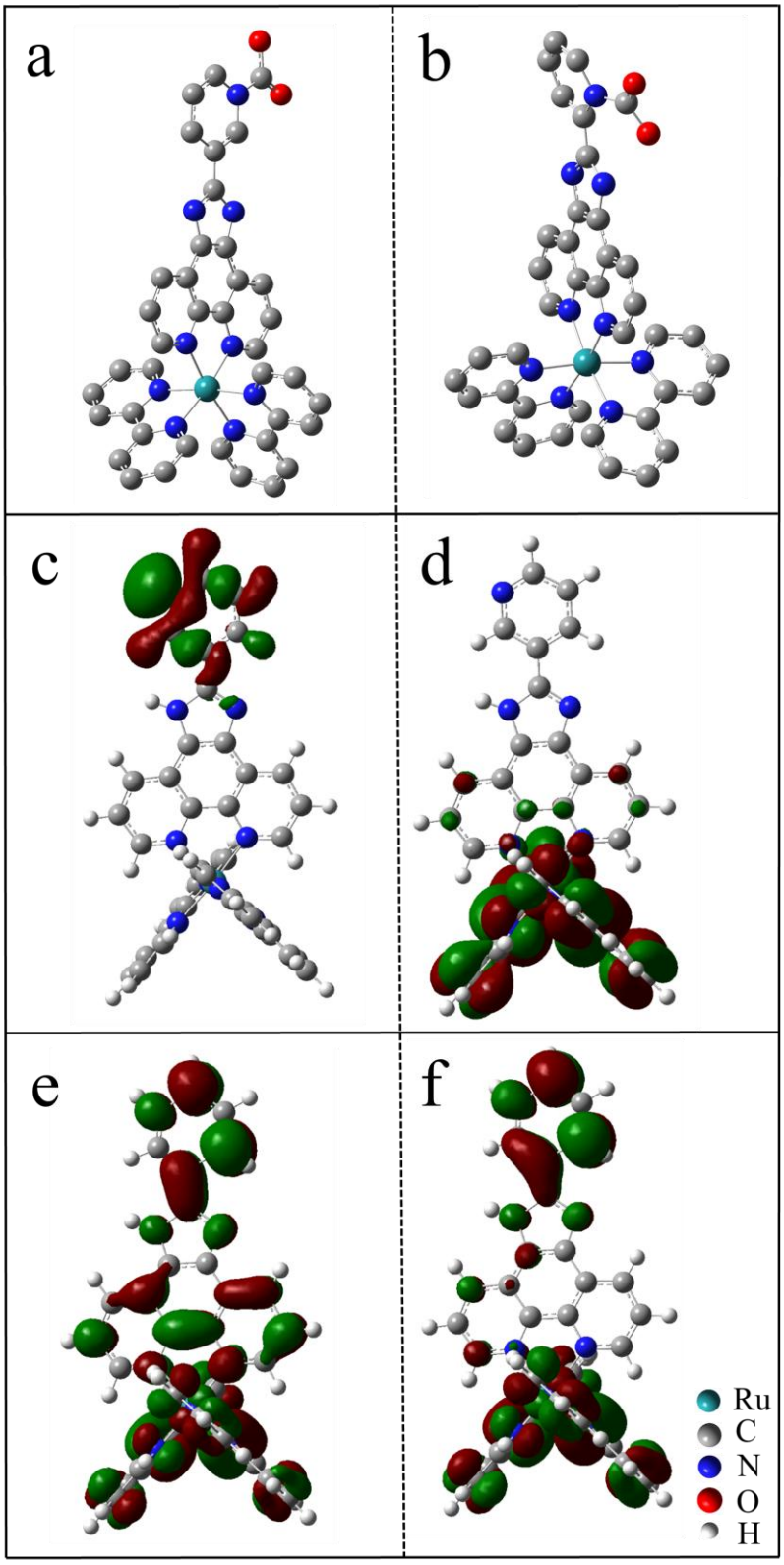

Scheme 1.

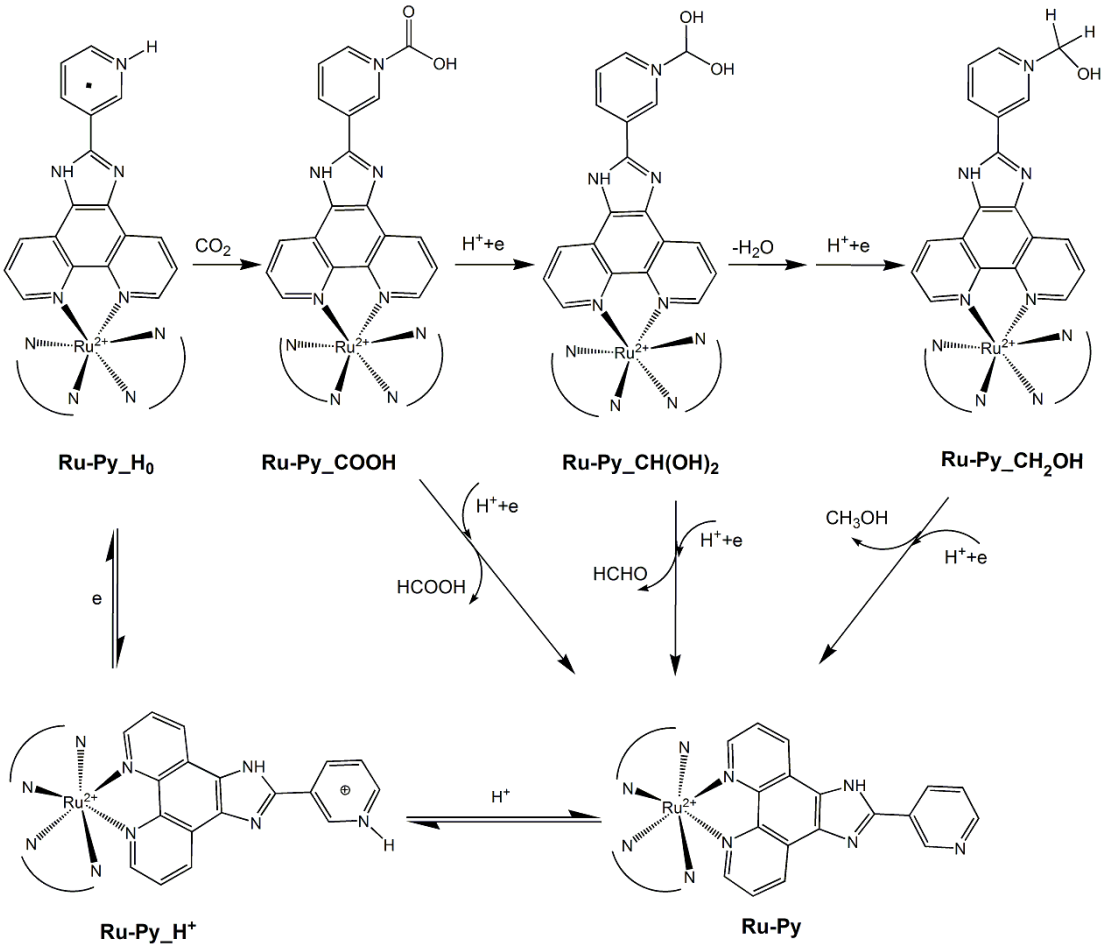

Table 1. Photo/Dark current compared to results presented in literatures.

| Catalyst | Condition | $\Delta j$/mAcm$^{-2}$[a] | Reference |
|---|---|---|---|
| Ru-Py | 0.1 M KCl, LA-410UV | 0.103 | this work |
| ZIF-9/CdS | MeCN/ $H_2O$ (v/v = 3/2), visable (>420 nm) | 0.015 | 24 |
| $Co_3O_4$ | 0.1 M $Na_2SO_4$, LA-410UV | -0.022 | 44, 48 |
| Pt/$TiO_2$ | 0.2MPa $CO_2$, $H_2O$, 200WXe lamp | 0.08 | 49 |
| UIO-66/CdS | 0.2 M $Na_2SO_4$, 300W Xe lamp | 0.020 | 50 |

a) $\Delta j$: The difference of the current with irradiation or not.

Table 2. TON and Faradic efficiency (f) compared to results presented in literatures.

| Electrode | pH | TON | $f_{MeOH}$(%) | $f_{total}$(%) | Referee |
|---|---|---|---|---|---|
| Ru-Py(FTO) | 5.0 | 6.4 | 27.3 | 83.1 | this work |
| p-GaP(EC) | 5.2 | - | 3.6 | | 30 |
| Cu/PdH(EC) | 5.2 | - | 15 | | 30 |
| Au(EC) | 5.0 | 2.5 | 22 | - | 31 |
| CdSe (PEC) | 5.0 | - | 0 | 60.7 | 32 |
| Pt(EC) | 5.2 | - | 14.5 | 33 | 55 |
| $CuInS_2$ (PEC) | 5.2 | 0.16 | - | - | 56 |

Values calculated based on information given in the reference. TON calculated based on Py catalyst.

Table 3. Conditions for controlled-potential electrolysis and MeOH production analyses.

| | pH | MeOH (μmol) | TON(in e) | $f_{MeOH}$(%) | $f_{total}$(%) |
|---|---|---|---|---|---|
| Ru-Py(PEC) | 4.0 | 11.2±1.8 | 2.9(17.8) | 12.5 | 55.6 |
| Ru-Py(PEC) | 5.0 | 24.1±2.1 | 6.4(38.4) | 27.3 | 83.1 |
| Ru-Py(PEC) | 6.0 | 6.2±0.9 | 1.6(9.6) | 10.9 | 62.4 |
| Ru-Py(EC) | 5.0 | 9.3±1.4 | 2.4(14.4) | 12.5 | 62.5 |
| Ru-Py (PC with AA)[a] | 5.0 | 2.7±0.8. | 0.70(4.2) | - | - |
| Ru-Py(PC) | 5.0 | 0.4±1.1 | 0.1(0.6) | - | - |
| Ru-Py(o)(PEC) | 5.0 | 14.3±2.8 | 3.7(22.2) | 16.9 | 79.9 |
| Ru-Ph(PEC) | 5.0 | 0.00 | 0.00 | 0 | 24.5 |
| Ru(II):Py(1:200)[b] | 5.0 | 3.6±0.8 | 0.9(5.4) | 9 | 48.5 |
| $Ru(phen)_3^{2+}$:Py(1:200)[c] | 5.0 | 1.7 | 0.3(1.8) | - | - |

a. AA: Ascorbic acid; b. Ru(II):Py: The Ru(II) photosensitizer and Py catalyst was not connected by C-C bond; c. Data from ref 38.